Anal. Bioanal. Electrochem., Vol. 17, No. 7, 2025, 583-600
https://www.doi.org/10.22034/abec.2025.729836

Analytical & Bioanalytical Electrochemistry

Full Paper

MOF Derived Bimetallic Ni/Co Phosphide-Nitride as Efficient Bifunctional Electrocatalyst for Overall Water Splitting

Noushin Hejr, Sedigheh Zeinali*, and Sayedeh Fatemeh Nami Ana

Nanochemical Engineering Department, Faculty of Advanced Technologies, Shiraz University, Shiraz, Iran

*Corresponding Author, Tel.: +987136139664
E-Mail: zeinali@shirazu.ac.ir

Received: 7 July 2025 / Received in revised form: 9 September 2025 / Accepted: 16 September 2025 / Published online: 30 September 2025

Abstract- A novel bifunctional electrocatalyst, bimetallic Ni/Co phosphide-nitride (BMNi/Co-NP), has been developed for efficient water splitting, targeting both hydrogen evolution reaction (HER) and oxygen evolution reaction (OER). This electrocatalyst was synthesized via low-temperature phosphidation of a porous Ni-rich cobalt-containing metal-organic framework (MOF). Characterization techniques, including XRD, FTIR, BET, and SEM, confirm the successful synthesis and structural integrity of the catalyst. The proposed electrocatalyst exhibits remarkable electrocatalytic performance with an overpotential of 270 mV for HER and 440 mV for OER at a current density of 10 mA cm^{-2}. The BMNi/Co-NP not only does it exhibits high catalytic activity, but it also demonstrates excellent stability, making it a promising candidate for large-scale clean energy applications. This research highlights the potential of MOF-derived materials in creating cost-effective, efficient electrocatalysts for sustainable hydrogen production.

Keywords- Hydrogen Evolution Reaction (HER); Oxygen Evolution Reaction (OER); Metal Organic Framework (MOF); Water splitting; Electrocatalysts; Nanostructured Catalysts

1. INTRODUCTION

The increasing global energy demand, along with the environmental damage caused by the widespread use of fossil fuels, has led to significant efforts to develop alternative clean energy sources. However, despite the progress in this active research area, renewable energy still

accounts for a small portion of the global energy supply due to challenges related to cost, safety, storage, and scalability [1].

Hydrogen, one of the simplest and most abundant elements, is considered a promising candidate for clean and sustainable energy. Unlike fossil fuels such as petroleum and natural gas, hydrogen is a clean-burning fuel whose only by-product is water. It can be used in various applications, including fuel cells (DFCs) [2–4]. Moreover, hydrogen has a high specific energy of approximately 283 kJ mol^{-1} and produces no harmful emissions during use [5–9].

Currently, several hydrogen production methods are available, such as steam methane reforming, coal gasification, biomass gasification, and water splitting through photoelectrochemical, electrochemical, and thermochemical processes [8]. Among these, electrochemical water splitting is considered one of the most promising approaches for renewable hydrogen generation [9,10]. This process involves two half-cell reactions: the hydrogen evolution reaction (HER) at the cathode and the oxygen evolution reaction (OER) at the anode. The overall water splitting reaction (Equation (1-1)) can be expressed as follows, including the corresponding half-reactions under different pH conditions (Equations (1-2) to (1-5)) [1].

$$2H_2O(aq) \rightarrow 2H_2(g) + O_2(g) \quad (1\text{-}1)$$

This reaction requires an input energy of approximately 237.1 KJ mol^{-1} (ΔG = 237.1 KJ mol^{-1}) under standard conditions, corresponding to a thermodynamic voltage of 1.23 V vs. RHE [11].

Hydrogen-evolution reaction:

$$2H^+(aq) + 2e^- \rightarrow H_2(g), \quad \text{(in acidic media)} \quad (1\text{-}2)$$

$$2H_2O(l) + 2e^- \rightarrow 2OH^-(aq) + H_2(g), \quad \text{(in alkaline media)} \quad (1\text{-}3)$$

Oxygen-evolution reaction:

$$2H_2O(l) \rightarrow O_2(g) + 4H^+(aq) + 4e^-, \quad \text{(in acidic media)} \quad (1\text{-}4)$$

$$4OH^-(aq) \rightarrow 2H_2O(l) + 4e^- + O_2(g), \quad \text{(in alkaline media)} \quad (1\text{-}5)$$

Hydrolysis, which involves breaking water bonds and forming hydrogen and oxygen molecules, is kinetically slow and requires a cell potential significantly higher than the thermodynamic value [1,12]. One of the main limitations in practical applications is the sluggish kinetics of the oxygen evolution reaction (OER), which typically exhibits higher overpotential (Za > Zc) due to its complex four-electron–proton coupled mechanism. In contrast, HER involves a simpler two-electron transfer process.

Among these two half-cell reactions, the anodic OER generally demands higher overpotential due to multiple elementary steps, including water adsorption and oxygen molecule formation. Although theoretically HER and OER should occur at 0 V and 1.23 V vs. RHE, respectively, in practice, due to kinetic limitations—especially HER in alkaline media

and OER in both acidic and alkaline conditions—the cell voltage of water electrolysis often exceeds 1.5 V, even with state-of-the-art electrocatalysts [13,14].

In real systems, electrochemical reactions rarely occur at their theoretical potentials unless all thermodynamic and kinetic constraints are addressed. Therefore, additional energy—known as overpotential (η) is required to initiate the reactions [1].

Identifying a suitable electrocatalyst capable of efficiently catalyzing both HER and OER simultaneously remains a major challenge. While many reported electrocatalysts exhibit high activity toward one of the two reactions, bifunctional catalysts that perform well for both are rare. Noble metals such as Pt (for HER) and Ir or Ru (for OER) offer excellent activity but suffer from high cost, scarcity, and poor long-term stability, limiting their industrial applicability. Thus, the development of high-performance bifunctional catalysts based on non-noble and earth-abundant metals is essential [10,15].

The Hydrogen Evolution Reaction (HER) in acidic conditions is straightforward due to the abundance of protons, proceeding through a multistep process via two possible mechanisms. The progress of HER can typically be analyzed using the Tafel plot slope (slope of Log|j| vs η plot), which can be experimentally obtained. The initial step in the multistep HER mechanism involves the discharge of protons on the electrode surface to form adsorbed hydrogen (H_{ads}), known as the Volmer reaction ($H^+(aq) + e^- \rightarrow H_{ads}$). Depending on the coverage of H_{ads}, the subsequent step is either the electrochemical desorption of H_2, referred to as the Heyrovsky reaction, or the Tafel reaction. Conversely, the Oxygen Evolution Reaction (OER) presents a different scenario. The kinetics of OER in acidic and alkaline media vary depending on the catalytic material used [1].

Recent studies have focused on designing electrocatalysts based on sulphides, selenides, and phosphides of transition metals such as WS_2 [16], MoS_2 [11], CoS_2 [17], $MoSe_2$ [18], $Co_{0.85}Se$ [19], $CoSe_2$ [20], Ni_2P [21], $Cu_{0.3}Co_{2.7}P$/NC [22], Ni-Fe-P [23], W_2N/WC [24], Co_2P [25], and NiFeCr-LDH/MoS_2 [26]. Among these, metal phosphides have shown excellent performance toward water splitting. Similarly, non-noble metals such as Co [27–30] and Ni [31–34] have demonstrated high catalytic activity. Both Ni and Co centers contribute to OER, while phosphorus enhances HER by modulating charge distribution and proton adsorption [11,15,35].

Over the past few decades, metal-organic frameworks (MOFs) have garnered significant attention in various fields, including gas storage, catalysis, sensing, and separation [36]. MOFs offer highly tunable porosity and abundant active sites, and their structures can be tailored by selecting different metals and ligands. In recent years, MOFs have been used directly as catalysts or indirectly as precursors for advanced electrocatalysts [36,37]. Thermal treatment of MOFs can convert their organic ligands into carbon and/or nitrogen-doped nanostructures, enhancing electrocatalytic activity [38, 39].

Here, a new approach has been used to introduce a robust and stable electrocatalyst, BMNi/Co-NP, as a new MOF, which acts as a bifunctional enhanced catalyst toward OER and HER with high efficiencies. The attractive capability of MOF structures has been used to construct a composite with both Ni and Co metals, which was shown remarkable properties. By choosing a suitable ligand (such as imidazolium-based ones) to design this bimetallic organic framework, N-doped Co based catalyst (BMNi/Co-N) can be easily made, which plays a positive role as electro-catalyst in the HER and OER reactions. Subsequently, the presence of phosphorus element next to BMNi/Co-N clearly has a positive improving effect on its electro-catalytic function. In this work, BMNi/Co-NP catalyst has been synthesized by low temperature phosphidation of the Ni-Co bimetallic organic frameworks which shows better performance as an electro-catalyst in both HER and OER reactions compared to both Ni-MOF and Co-MOF catalysts. This effect may be related to the strong synergistic effects in the bimetallic Ni-Co system [38,39]. Using the proposed electro-catalyst, BMNi/Co-NP, overpotential of 270 mV at 10 $mA \cdot cm^{-2}$ and Tafel slope of 82.9 mV per decade were obtained for HER reactions. Also, the overpotential of 440 mV at 10 $mA \cdot cm^{-2}$ and Tafel slope of 71.6 mV per decade were obtained for OER reactions. Therefore, we leverage the unique composition and structure of Ni-Co bimetallic materials and the non-metallic phosphide imidazolate-based framework with good results which is better or comparable to most of electro-catalyst with similar compositions previously reported [19,24,36–45].

To the best of our knowledge, there is no report on using this kind of electro-catalyst in HER and OER reactions yet.

In recent years (2024–2025), significant progress has been achieved in the development of bifunctional electrocatalysts for both the hydrogen evolution reaction (HER) and the oxygen evolution reaction (OER). A major focus of this progress has been the utilization of metal–organic frameworks (MOFs) and MOF-derived materials, which have shown notable improvements in both efficiency and long-term stability in green hydrogen production systems.

Furthermore, recent studies have highlighted the potential of MOF-derived and bimetallic nanostructures for overall water splitting. For instance, a NS-RGO-Cu-MOF composite has been reported as an efficient bifunctional electrocatalyst for both HER and OER [46,47]. Another study introduced a copper-based MOF integrated with nitrogen and sulfur dual-doped graphene oxide, which exhibited promising performance in oxygen reduction reactions [48]. These advances underline the relevance and novelty of the BMNi/Co-NP catalyst developed in this study, which builds upon recent trends in MOF-derived multifunctional materials for efficient water splitting.

2. EXPERIMENTAL SECTION

2.1. Reagents and instrumentation

All reagents, including nickel nitrate hexahydrate ($Ni(NO_3)_2 \cdot 6H_2O$), cobalt nitrate hexahydrate ($Co(NO_3)_2 \cdot 6H_2O$), 2-methylimidazole ($C_4H_6N_2$), N,N-dimethylformamide (DMF), sodium hypophosphite (NaH_2PO_2), and ethanol, were of analytical grade and purchased from Merck (Darmstadt, Germany). Nafion (5 wt.%) was obtained from Sigma-Aldrich. All chemicals were used as received without further purification.

2.2. Preparation of Metal organic frameworks

2.2.1. Synthesis of ZIF-67 and Ni-MOF

The synthesis of Co-MOFs (ZIF-67) was performed using a previously reported method [40], involving the mixing of cobalt nitrate hexahydrate and 2-methylimidazole (Hmim) to produce purple precipitates. For the synthesis of Ni-MOF, 0.9 g of $Ni(NO_3)_2 \cdot 6H_2O$ was dissolved in a solvent mixture of DMF, ethanol, and deionized water (1:1:1 v/v/v; total volume: 4 mL). Separately, 3.7 g of Hmim was dissolved in 16 mL of the same solvent mixture under constant stirring until a clear solution was obtained. The two solutions were then combined and stirred for several minutes to form a homogeneous ink. This mixture was transferred to a 50 mL Teflon-lined stainless-steel autoclave and heated at 120 °C for 24 h. After cooling to room temperature, the resulting precipitate was collected by centrifugation at 6000 rpm for 15 minutes, washed four times with DMF and ethanol, and subsequently dried at 60 °C for 17 hours.

2.2.2. Synthesis and phosphidation of bimetallic BMNi/Co-NP

In brief, to prepare the Ni/Co-rich textured products, $Co(NO_3)_2 \cdot 6H_2O$ and $Ni(NO_3)_2 \cdot 6H_2O$ were dissolved in a mixed solvent of DMF, ethanol, and water at a 1:1:1 (v/v/v) ratio (total volume 4 mL). Four different samples were prepared with varying Co:Ni molar ratios, designated as Ni/Co-MOF(n) (Co:Ni = 1:n, where n = 1, 2, 3, 4). Subsequently, 3.7 g of Hmim was dissolved in 16 mL of the same solvent mixture under stirring until the solution became clear. A similar procedure was followed to continue the synthesis.

For the phosphidation of the bimetallic Ni/Co-MOF, the pre-synthesized Ni/Co-MOF and sodium hypophosphite (NaH_2PO_2) with a mass ratio of 1:10 were placed separately in an alumina boat. The boat was then inserted into a quartz tube furnace under an argon atmosphere, heated to 350 °C at a ramp rate of 5 °C/min, and maintained at this temperature for 3 hours. Finally, the resulting black powder was collected.

2.3. Apparatus

2.3.1. Materials characterization

The crystalline structure of the synthesized MOFs was characterized using a Bruker D8 Advance X-ray diffractometer with copper radiation (Cu Kα, λ = 0.15418 nm, 40 kV / 40 mA,

and a scanning rate of 3°/min). Scanning electron microscopy (SEM) was performed using a TESCAN VEGA3 microscope at an accelerating voltage of 30 kV, with the samples coated by a DSR nanostructure coater to examine the morphology and structure. Elemental analysis was conducted using energy dispersive spectroscopy (EDS). Fourier-transform infrared (FTIR) spectra were recorded with a BRUKER Tensor II infrared spectrophotometer. Brunauer–Emmett–Teller (BET) analysis was employed to investigate the properties of the samples, specifically Ni/Co-MOF(3) and BMNi/Co-NP textures, using N_2 adsorption/desorption on a Micromeritics ASAP 2020 instrument.

2.3.2. Electrochemical measurements

Electrochemical measurements, including linear sweep voltammetry (LSV) and cyclic voltammetry (CV), were performed using an Autolab (PGSTAT302N) system with a three-electrode setup. Hydrogen evolution reaction (HER) measurements were carried out in N_2-saturated 0.5 M sulfuric acid solution, while oxygen evolution reaction (OER) measurements were conducted in N_2-saturated 1 M potassium hydroxide solution at room temperature.
To prepare the working electrode, 5 mg of electrocatalyst powder was dispersed in 1 mL of a deionized water:ethanol mixture (3:1 v/v), and 30 µL of Nafion solution (5% w/w in water and 1-propanol) was added. The suspension was sonicated in an ultrasonic bath for 20 minutes to obtain a homogeneous ink. Then, 5 µL of the ink was drop-cast onto a glassy carbon (GC) electrode (2 mm diameter) and dried. A platinum wire served as the counter electrode, and an Ag/AgCl electrode was used as the reference electrode. All measured potentials were converted to the reversible hydrogen electrode (RHE) scale according to the Nernst equation ($E_{RHE} = E_{Ag/AgCl} + 0.197 + 0.059\ pH$) [41].

3. RESULTS AND DISCUSSION

3.1. Characterization

3.1.1. ZIF-67, Ni-MOF and Ni/Co-MOFs

SEM images of ZIF-67 crystals were collected to obtain a comprehensive understanding of their morphology (Figure S1A). The images show that the synthesized ZIF-67 crystals have a regular polygonal shape with well-defined faces and straight edges. The average particle size of ZIF-67 is approximately 188 nm.

To investigate the crystalline structure of the synthesized ZIF-67, powder X-ray diffraction (XRD) analysis was performed. The XRD pattern of ZIF-67 (Figure S1B) shows three strong peaks located at $2\theta = 7.35°$, 12.85°, and 18.15°, corresponding to the (011), (112), and (222) crystal planes, respectively, which are in good agreement with the reported simulation [40]. The pronounced and well-defined peaks indicate the high crystallinity of the synthesized ZIF-67 crystals.

One of the most important advantages of using MOF templates for catalyst preparation is the construction of a porous structure containing different metal nodes with electrocatalytic capabilities. Typical SEM images were taken to investigate the morphologies and microstructural details of the synthesized Ni-MOF and bimetallic Ni/Co-MOF samples (Figure S2). As mentioned previously, different bimetallic MOFs composed of Ni and Co were prepared at various Ni:Co ratios. At equal amounts of Ni and Co, nanosheet structures of the bimetallic MOFs were observed (Figures S2A, B). As evident, by increasing the nickel content, fibroid structures begin to emerge within the morphology (Figures S2C–H). It appears that the structure of Ni/Co-MOF changes with increasing Ni content, resulting in a morphology that is a combination of nanosheets and nanofibers. The SEM images of Ni-MOF can also be seen in Figures S2I, J.

Elemental composition of the different synthesized structures was determined by EDS analysis. Typical EDS analyses of Ni/Co-MOF(1) and Ni/Co-MOF(3) are shown in Figures S4 and S5. The SEM-EDS elemental mapping confirms the uniform distribution of the elements.

The crystallinity of Ni-MOF and Ni/Co-MOFs was investigated by XRD. Figure S3 shows comparable XRD patterns for Ni/Co-MOF(1), Ni/Co-MOF(3), and Ni-MOF. It is apparent that Ni-MOF exhibits a relatively amorphous structure compared to the crystalline bimetallic Ni/Co-MOFs. By comparing the XRD patterns with those of ZIF-67, it can be concluded that the crystalline structure of Ni/Co-MOFs may be intermediate between those of Ni-MOF and ZIF-67.

3.1.2. BMNi/Co-NP

As mentioned previously (Section 2.2.2), the bimetallic BMNi/Co-MOF was phosphidated to enhance its electrocatalytic properties. The prepared phosphidated samples, BMNi/Co-NP, were characterized using various techniques.

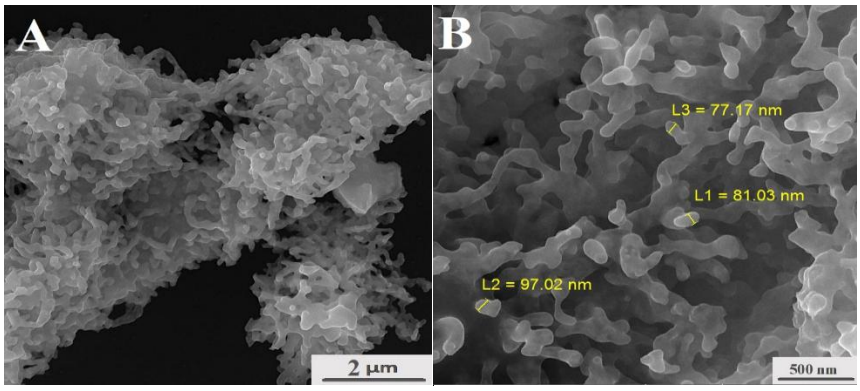

Figure 1. FE-SEM images (A, B)

In the SEM images (Figures 1A, B), it can be observed that the fibroid structure transformed into a coral-like morphology after the phosphidation process, with the original morphology

well preserved. To understand how the Ni and Co phosphides were attached to the surface of the Ni/Co-MOF, EDS mapping was performed and is shown in Figure S6. The EDS analysis revealed the coexistence of C, O, N, Ni, Co, and P with the mentioned mass fractions.

The XRD pattern of the synthesized BMNi/Co-NP after phosphidation under Ar flow is shown in Figure 2. The diffraction peaks at 2θ = 40.85°, 44.82°, 47.49°, and 54.35° can be indexed to the (111), (210), and (300) planes of hexagonal NiCoP (JCPDS No. 71-2336).

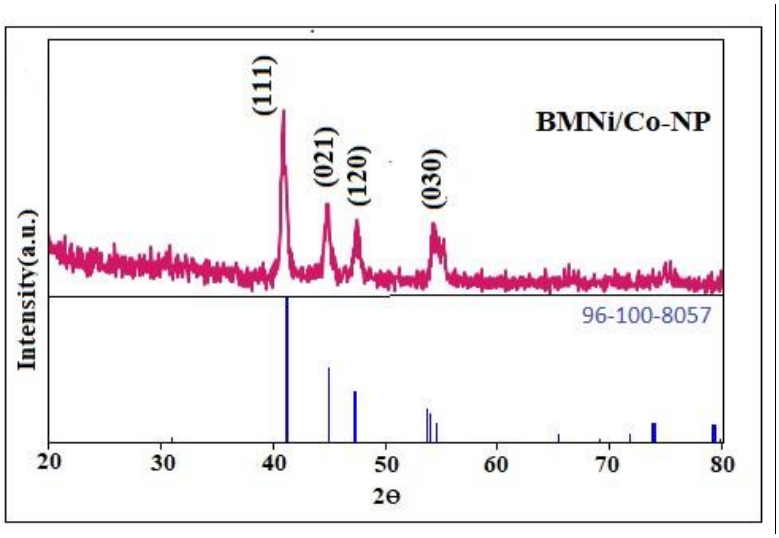

Figure 2. XRD pattern of the BMNi/Co-NP

FTIR spectra of the pre-synthesized MOFs as electrocatalysts were collected, and the results are shown in Figure 3. One of the most important evidences for framework formation is the absence of the peak at 1844 cm^{-1}, which corresponds to the stretching vibration of the N–H group in 2-methylimidazole [42]. The disappearance of this peak can be attributed to the coordination of Co^{2+} ions, which alters the vibration frequencies due to framework formation. The peak observed around 1578 cm^{-1} corresponds to aromatic C=H stretching, while the peak at 1300 cm^{-1} represents the vibrational mode of the C-H bond in the ZIF-67 structure. The stretching vibration of Co–N can be observed at 425 cm^{-1} [43]. A small peak at 3135 cm^{-1} refers to the stretching of C–H from the aromatic ring of the 2-methylimidazole linker. Multiple peaks in the range of 1500–600 cm^{-1} indicate the stretching and bending vibrations of the imidazole group [44]. The main peaks of ZIF-67 are also present in Ni/Co-MOF. Only a few new peaks appear in the Ni/Co-MOF(3) spectrum. For example, the relatively broad band at 2928 cm^{-1} corresponds to the stretching vibration of aliphatic C–H of 2-methylimidazole, which has shifted from 3100 cm^{-1} (in pure 2-methylimidazole) due to strong interactions with Ni^{2+} ions [49].

In the FTIR spectrum of BMNi/Co-NP (Figure 1D), two bands near 544 cm^{-1} and 578 cm^{-1} appear within the 560–604 cm^{-1} range, corresponding to P–O bonds. The peak near 950 cm^{-1}

is also related to P–O vibrations, while the band observed near 1145 cm^{-1} corresponds to P=N bonds.

The BET analysis results shown in Figure S7 indicate that after phosphidation of Ni/Co-MOF(3), the BET surface area slightly decreased to 172.4 m^2/g. Additionally, the pore size increased slightly to 7.2 nm. The mesoporous nature of the compounds is evident from the hysteresis observed in the isotherm diagram.

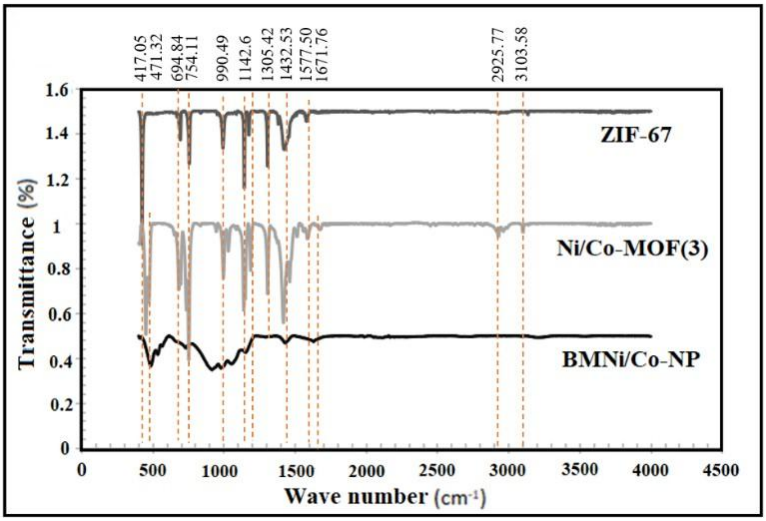

Figure 3. FT–IR spectra of ZIF-67, Ni/Co-MOF and BMNi/Co-NP

3.2. Electrochemical measurements

3.2.1. HER activity

Firstly, the electrocatalytic activities of the as-prepared cobalt-based catalysts for the hydrogen evolution reaction (HER) were evaluated using steady-state linear sweep voltammetry (LSV) in an N_2-saturated 0.5 M H_2SO_4 solution (Figure 4). The HER electrocatalytic performance of the porous BMNi/Co-NP was compared with ZIF-67, Ni-MOF, and Ni/Co-MOFs to investigate the synergistic effects of all components. As expected, the synthesized ZIF-67 exhibited notable HER activity; however, an overpotential of 670 mV was required to achieve a current density of 10 mA cm^{-2}. Ni/Co-MOF(3) demonstrated improved HER activity due to the presence of nickel. Furthermore, the phosphidation of Ni/Co-MOF to form the BMNi/Co-NP framework resulted in a significant enhancement in HER activity. The BMNi/Co-NP showed superior HER performance in 0.5 M H_2SO_4 compared to the other catalysts (Figure 4). It can be concluded that the incorporation of cobalt, nickel, and phosphorus within a porous structure led to a remarkable catalytic enhancement. The synthesized BMNi/Co-NP exhibited exceptionally high activity with a low onset potential of approximately 84 mV (Figure 1A, B). An overpotential of 270 mV was required to reach a HER current density of 10 mA cm^{-2}.

In comparison, commercial platinum-based catalysts typically demand significantly lower overpotential values—approximately 30–50 mV under similar acidic conditions. Although the BMNi/Co-NP exhibits a higher overpotential than Pt, its advantages in terms of cost efficiency, abundance of constituent metals, and excellent electrochemical stability make it a promising candidate for practical and scalable hydrogen evolution applications [50]. The Tafel curve of BMNi/Co-NP (Figure 4C) was plotted, and a slope of approximately 82.9 mV dec^{-1} was obtained from the extrapolation of the linear region of overpotential (η) versus log j. This Tafel slope is significantly lower than those of ZIF-67 (104 mV dec^{-1}), Ni-MOF (162 mV dec^{-1}), and Ni/Co-MOFs (97, 114, 115, and 106 mV dec^{-1} for Ni/Co-MOF(1), Ni/Co-MOF(2), Ni/Co-MOF(3), and Ni/Co-MOF(4), respectively). Such a low Tafel slope for BMNi/Co-NP suggests highly efficient hydrogen evolution kinetics, consistent with a two-electron transfer process following the Volmer–Heyrovsky mechanism involving bimolecular adsorption and hydrogen evolution [38].

In addition to electrocatalytic activity, stability is a critical parameter for evaluating electrocatalysts, especially when assessing their practical application potential. Therefore, the electrochemical stability and durability of BMNi/Co-NP toward HER were investigated using cyclic voltammetry (CV), linear sweep voltammetry (LSV), and chronoamperometry techniques.

The initial LSV before the CV scan and the final LSV after 1000 CV cycles were compared and overlaid in Figure 4D. As shown in Figure 4D, BMNi/Co-NP exhibits negligible loss in current density after 1000 CV cycles. The CV was recorded at a scan rate of 100 mV s^{-1}, which is relatively fast. Durability was also evaluated by chronoamperometry (at applied potential -0.390 V vs RHE), with the results presented in Figure 4E. As evident, the electrocatalyst maintains a steady current density of 10 mA cm^{-2} during continuous operation for 10 hours.

After 1000 CV cycles, 8.1% decrease in current density was observed. Additionally, in the chronoamperometry test over 10 hours, the BMNi/Co-NP catalyst maintained a steady current density of 10 mA cm^{-2}. These results demonstrate the outstanding stability of the catalyst compared to commercial catalysts such as Pt, which shows a 15% decrease in current density after 1000 CV cycles. Therefore, the BMNi/Co-NP catalyst, with its excellent stability and cost efficiency, shows significant potential for industrial applications.

To further evaluate the intrinsic catalytic activity of the synthesized BMNi/Co-NP electrocatalyst toward the hydrogen evolution reaction (HER), the mass-normalized turnover frequency (TOF) was calculated. TOF represents the number of hydrogen molecules generated per geram of catalyst per second, providing a more fundamental insight into the catalyst efficiency beyond current density and overpotential values. Ultimately, the TOF value was calculated using the following formula:

$$\frac{I}{nF \times m} = {}_{\text{mass}}\text{TOF}$$

where ***I*** is the current at 10 mA cm^{-2} (converted to A), ***F*** is the Faraday constant (96485 C mol^{-1}), and ***n*** Number of electrons involved in the formation of one molecule of product (for HER, n=2), and ***m*** is Mass of the catalyst loaded on the electrode. [51]

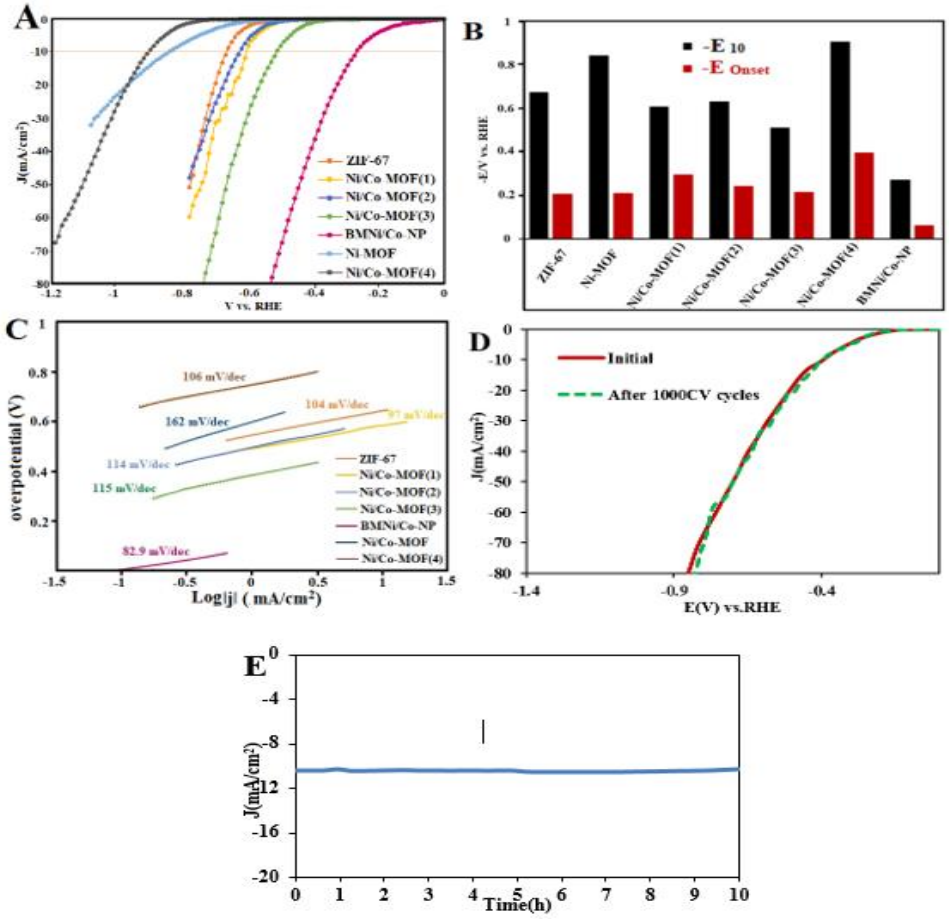

Figure 4. LSV curves for all proposed electrocatalysts measured in N_2-saturated 0.5 M H_2SO_4 solution at a scan rate of 10 mV s^{-1}. (A) Histograms comparing the onset potential (E_onset) and overpotential at 10 mA cm^{-2} (η@10) values for the hydrogen evolution reaction (HER). (B) Tafel plots derived from the LSV curves for ZIF-67, Ni-MOF, Ni/Co-MOF samples (1–4), and BMNi/Co-NP. (C) LSV curves recorded before and after 1000 cyclic voltammetry (CV) cycles under identical conditions. (D) Chronoamperometry test of BMNi/Co-NP at a constant current density of 10 mA cm^{-2} over 10 hours (E). All measurements were conducted at room temperature under N_2-saturated conditions. BMNi/Co-NP exhibits superior catalytic performance across all conditions compared to other catalysts

The TOF was estimated in this study. a catalyst with an exceptionally low loading (~7.85 $\times 10^{-7}$ g) was synthesized and evaluated for its electrocatalytic performance in hydrogen evolution reaction (HER) and oxygen evolution reaction (OER). Despite the minimal mass, the catalyst demonstrated remarkable turnover frequencies (TOF), at an overpotential

corresponding to a current density of 10 mA cm^{-2}, reaching approximately 81.6 mol/s/g. These values surpass those of many benchmark catalysts, including noble-metal-based systems such as Pt/C. [52]

This high TOF value demonstrates that BMNi/Co-NP possesses excellent intrinsic catalytic activity toward HER, outperforming many benchmark catalysts reported in the literature. The results confirm that the synergistic effect of bimetallic Ni/Co phosphide-nitride composition, combined with the porous structure, significantly enhances the number and activity of catalytic sites.

3.2.2. OER activity

The electrocatalytic OER activity of the prepared electrocatalysts was also examined using a three-electrode system. Figure 5A shows the anodic polarization curves of BMNi/Co-NP at a scan rate of 10 mV s^{-1} in 1.0 M KOH solution. The OER activity of porous BMNi/Co-NP was compared with that of ZIF-67, Ni-MOF, and Ni/Co-MOFs in N_2-saturated 1 M KOH solution. The results showed that ZIF-67, Ni-MOF, and Ni/Co-MOFs exhibited similarly poor OER activities, while BMNi/Co-NP proved to be a promising catalyst for OER.

Transition metal phosphides have previously been demonstrated as highly effective catalysts for OER [53]. Studies on single metal phosphides have shown that Co-P exhibits even better activity than commercial RuO_2, which is considered the benchmark catalyst for OER [54,55]. The BMNi/Co-NP material, as a preferred OER electrocatalyst, demonstrated excellent catalytic performance with a remarkably low onset potential of approximately 200 mV. Among all the synthesized samples, BMNi/Co-NP exhibited the lowest onset potential and the highest catalytic activity for OER. An overpotential of 440 mV is required to achieve an OER current density of 10 mA cm^{-2}, which is competitive with the benchmark RuO_2 catalyst that typically exhibits an overpotential in the range of 350–400 mV under similar conditions [56]. Considering the lower cost and enhanced stability of BMNi/Co-NP compared to noble metal-based catalysts, this result highlights its potential as an efficient and economically viable alternative for OER applications.

The electrocatalytic OER kinetics of BMNi/Co-NP were assessed using the Tafel slope, derived from the linear region of the Tafel plot by fitting the experimental data to the Tafel equation ($\eta = b \log j + a$, where η is the overpotential, j is the current density, and b is the Tafel slope). The Tafel curve (Figure 5B) for BMNi/Co-NP shows a slope as low as 71.6 mV dec^{-1}, which is significantly lower than those of the other catalysts (Figure 5B).

Based on the definition and formula of turnover frequency (TOF), and considering that the oxygen evolution reaction (OER) involves the transfer of four electrons (n = 4), the calculated TOF for this reaction is 40.8 $mol \cdot s^{-1} \cdot g^{-1}$. This value reflects the high intrinsic activity of the catalyst and is comparable to the performance of benchmark noble-metal-based catalysts [52].

Also, as reported, the number of MOFs stable in strong alkaline solutions is quite limited, and examples of stable MOFs exhibiting electrocatalytic activity toward OER are relatively

rare [57]. Therefore, the exceptional durability of this new catalyst represents a significant advancement for oxygen evolution in alkaline media. Not only is catalytic activity toward OER important, but the excellent durability of the electrocatalyst is also a critical criterion for all energy conversion systems. The durability of the electrocatalyst was evaluated by recording LSV before and after 1000 consecutive CV scans and comparing the results, as shown in Figure 5C, which indicates no significant loss in current density. The long-term stability of BMNi/Co-NP was further assessed using chronoamperometry at 1.75 V *vs.* RHE, as shown in Figure 5D. The current density of 10 mA cm^{-2} remained nearly constant for at least 10 hours, with only a minor decrease of about 3%. This result demonstrates the electrocatalyst's excellent stability under harsh conditions.

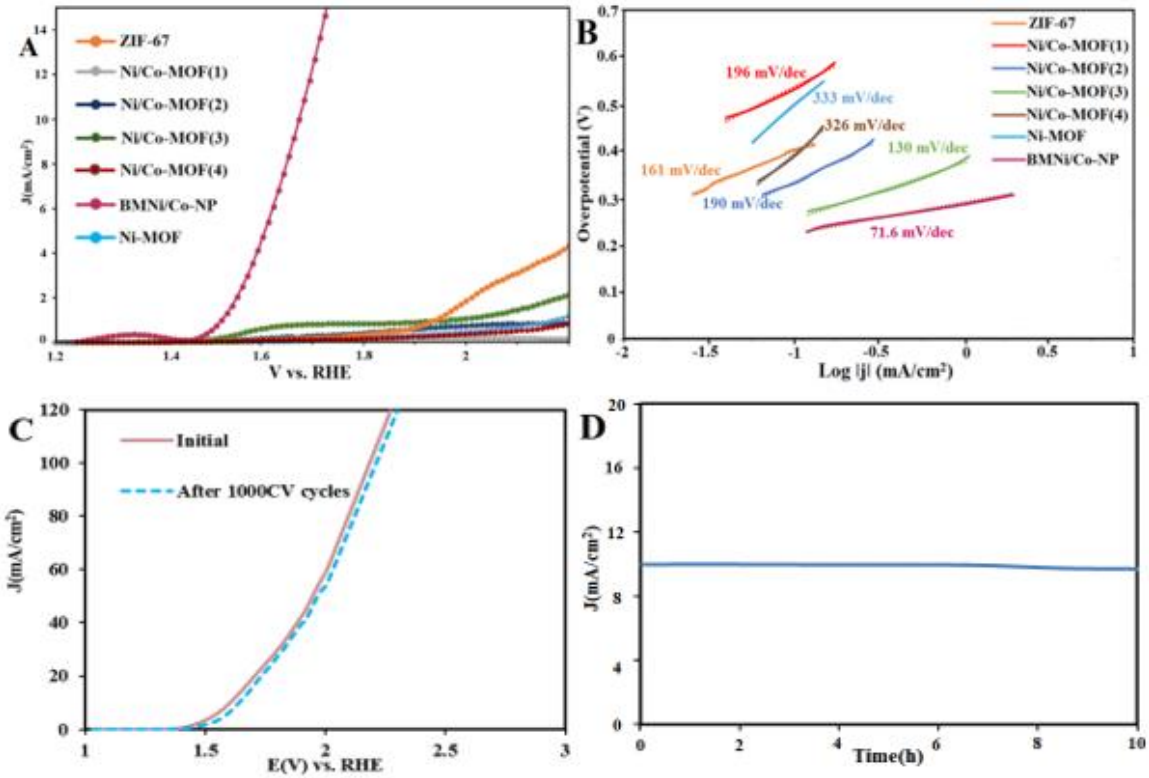

Figure 5. Electrocatalytic oxygen evolution reaction (OER) performance of BMNi/Co-NP compared to other catalysts in N_2-saturated 1.0 M KOH at room temperature.Anodic polarization curves at a scan rate of 10 mV s^{-1} showing a low onset potential (E_onset ≈ 200 mV) and an overpotential of 440 mV to reach 10 mA cm^{-2} (η@10) for BMNi/Co-NP (A); Tafel plots with a slope of 71.6 mV dec^{-1}, indicating faster reaction kinetics (B); Stability test after 1000 CV cycles showing no significant performance loss (C); Long-term chronoamperometric stability with nearly constant current density over 10 hours (D)

There are several reports indicating that the incorporation of phosphorus (P) into the structure of electrocatalysts can improve their performance toward OER and HER. For example, Y. Pan et al. [58] reported nanocrystalline Ni_5P_4 for OER and discussed the effects

of in-situ P incorporation on the surface reconstruction of NiO for OER electrocatalysis. Using theoretical calculations, they revealed that P substitution for O atoms in the nickel oxide (NiO) structure weakens the binding strength of OER intermediates such as *OH, *O, and *OOH, thereby altering the potential-determining step of OER and consequently achieving a lower theoretical overpotential. They also presented charge density diagrams, stating that doping with P atoms leads to electron accumulation around Ni, promoting adsorption of the intermediates. H. Hu et al. [59] proposed a possible mechanism at the NiCoP–CoP interface for water splitting. They stated that *OH− has a higher tendency to adsorb on the Ni site in alkaline solution, whereas H atoms prefer the Co site and convert into adsorbed H (*H). Therefore, the presence of CoP in NiCoP–CoP heterostructures provides suitable sites for timely H adsorption, thus improving HER performance. A comparison between this work and some similar studies is presented in Table 1 to illustrate the performance of the proposed electrocatalyst.

Table 1. Comparison of performance for different electrocatalysts for HER and OER

Electrocatalyst	Electrolyte	Reaction	Overpotential(@10mA/cm^2) (mV)	Tafel slope mV/dec	Scan rate (mV/S)	Ref.
BMNi/Co-NP	0.5 M H_2SO_4	HER	270	82.9	10	This work
	1 M KOH	OER	440	71		
W_2N/WC heterostructures	0.5 M H_2SO_4	HER	148.5	47.4	5	[24]
Co_2P	0.5 M H_2SO_4	HER	190	61	5	[25]
	1 M KOH	OER	364	78	1	
TCNC	0.5 M H_2SO_4	HER	290	110	10	[25]
	1 M KOH		300	133		
NiFe-LDH/Ni foam	1 M KOH	OER	450	72	10	[60]
MoS_2	0.5 M H_2SO_4	HER	260	85	10	[61]
Co_3O_4@CNT composite	1 M KOH	OER	470	76	10	[62]

4. CONCLUSION

The creation of the bimetallic Ni/Co phosphide-nitride (BMNi/Co-NP) as a bifunctional electrocatalyst represents a major breakthrough in water splitting technology. This study successfully demonstrates that BMNi/Co-NP exhibits exceptional electrocatalytic performance for overall water splitting, achieving low overpotentials of 270 mV and 440 mV at a current density of 10 mA cm^{-2} for HER and OER, respectively. The synthesis process, utilizing a low-temperature phosphidation of Ni-rich cobalt-containing metal-organic frameworks, showcases

the potential of MOFs as precursors for high-performance electrocatalysts. The findings highlight the synergistic effects of the bimetallic composition and the incorporation of phosphorus, which enhance the catalytic activity and stability of the electrocatalyst. The BMNi/Co-NP not only outperforms traditional catalysts but also presents a cost-effective alternative, addressing the challenges of scalability and sustainability in clean energy production.

The roles of Ni, Co, and P in the catalytic enhancement of the BMNi/Co-NP electrocatalyst are essential for understanding the observed synergy in hydrogen and oxygen evolution reactions (HER and OER). As mentioned briefly, the Volmer–Heyrovsky mechanism is relevant for HER, where Ni and Co atoms act as active centers for the hydrogen adsorption and desorption steps, while phosphorus atoms play a key role in promoting hydrogen evolution by stabilizing adsorbed intermediates such as *H. The phosphide phase (Ni-Co-P) has been shown to provide enhanced electronic interactions, which lower the overall activation energy required for the reaction. For OER, the Co and Ni metal centers contribute to the activation of water molecules and the formation of oxygen intermediates, while P stabilizes the transition states and accelerates the oxygen evolution steps. These interactions are crucial for understanding the high catalytic efficiency of BMNi/Co-NP.

In conclusion, the promising results of this study pave the way for further exploration and optimization of MOF-derived electrocatalysts, potentially accelerating the transition towards renewable hydrogen production and contributing to global efforts in sustainable energy solutions. Future research should focus on the long-term stability and practical applications of BMNi/Co-NP in real-world electrochemical systems.

Acknowledgements

We acknowledge Shiraz University as providers of financial sum, facilities, contributors, etc.

Declarations of interest

The authors declare no conflict of interest in this reported work.

REFERENCES

[1] S. Anantharaj, S. Rao Ede, K. Sakthikumar, K. Karthick, S. Mishra, and S. Kundu, ACS Catal. 6 (2016) 8069.

[2] A.V. Churikov, A.V. Ivanishchev, I.M. Gamayunova, and A.V. Ushakov, J. Chem. Eng. Data 56 (2011) 3984.

[3] A.V. Churikov, K.V. Zapsis, A.V. Ivanishchev, and V.O. Sychova, J. Chem. Eng. Data 56 (2011) 2543.

[4] A.V. Churikov, I.M. Gamayunova, K.V. Zapsis, M.A. Churikov, and A.V. Ivanishchev, Int. J. Hydrogen Energy 37 (2012) 335.
[5] H. Ogihara, M. Fujii, and T. Saji, RSC Adv. 4 (2014) 15860.
[6] D. Das, S. Santra, and K. Nanda, ACS Appl. Mater. Interfaces 10 (2018) 35025.
[7] S. Shit, S. Chhetri, W. Jang, N.C. Murmu, H. Koo, P. Samanta, and T. Kuila, ACS Appl. Mater. Interfaces 10 (2018) 27712.
[8] M. El-Shafie, S. Kambara, and Y. Hayakawa, J. Power Energy Eng. 7 (2019) 107.
[9] A. Choedel, Z. Ji, and O.M. Yaghi, Nat. Energy 1 (2016) 16034.
[10] F. Zhang, Y. Ge, H. Chu, P. Dong, R. Baines, Y. Pei, M. Ye, and J. Shen, ACS Appl. Mater. Interfaces 10 (2018) 7087.
[11] J.D. Benck, T.R. Hellstern, J. Kibsgaard, P. Chakthranont, and T.F. Jaramillo, ACS Catal. 4 (2014) 3957.
[12] J. Masud, A.T. Swesi, W.P.R. Liyanage, and M. Nath, ACS Appl. Mater. Interfaces 8 (2016) 17292.
[13] M. Tahir, L. Pan, F. Idrees, X. Zhang, L. Wang, J.J. Zou, and Z.L. Wang, Nano Energy 37 (2017) 136.
[14] Y. Zhang, X. Wang, J. Li, and Y.C. Chen, J. Mater. Chem. A 10 (2022) 8500.
[15] J. Bai, T. Meng, D. Guo, S. Wang, B. Mao, and M. Cao, ACS Appl. Mater. Interfaces 10 (2018) 1678.
[16] M.A. Lukowski, A.S. Daniel, C.R. English, F. Meng, A. Forticaux, R.J. Hamers, and S. Jin, Energy Environ. Sci. 7 (2014) 2608.
[17] M.S. Faber, R. Dziedzic, M.A. Lukowski, N.S. Kaiser, Q. Ding, and S. Jin, J. Am. Chem. Soc. 136 (2014) 10053.
[18] H. Wang, D. Kong, P. Johanes, J.J. Cha, G. Zheng, K. Yan, N. Liu, and Y. Cui, Nano Lett. 13 (2013) 3426.
[19] S. Li, S. Peng, L. Huang, X. Cui, A.M. Al-Enizi, and G. Zheng, ACS Appl. Mater. Interfaces 8 (2016) 20534.
[20] K. Zhou, J. He, X. Wang, J. Lin, Y. Jing, W. Zhang, and Y. Chen, Electrochim. Acta 231 (2017) 626.
[21] E.J. Popczun, J.R. McKone, C.G. Read, A.J. Biacchi, A.M. Wiltrout, N.S. Lewis, and R.E. Schaak, J. Am. Chem. Soc. 135 (2013) 9267.
[22] J. Song, C. Zhu, B.Z. Xu, S. Fu, M.H. Engelhard, R. Ye, D. Du, S.P. Beckman, and Y. Lin, Adv. Energy Mater. 6 (2016) 1601555.
[23] S.H. Ahn and A. Manthiram, J. Mater. Chem. A 5 (2017) 2496.
[24] J. Diao, Y. Qiu, S. Liu, W. Wang, K. Chen, H. Li, W. Yuan, Y. Qu, and X. Guo, Adv. Mater. 32 (2020) 1905679.
[25] J. Jebaslinhepzybai, B. Thangadurai, T. Partheeban, D.S. Gavali, R. Thapa, and M. Sasidharan, Int. J. Hydrogen Energy 46 (2021) 21924.

[26] S. Chen, C. Yu, Z. Cao, X. Huang, S. Wang, and H. Zhong, Int. J. Hydrogen Energy 46 (2021) 7037.
[27] Z. Zhou, N. Mahmood, Y. Zhang, L. Pan, L. Wang, X. Zhang, and J. Zou, J. Energy Chem. 26 (2017) 1223.
[28] J. Lin, J. He, F. Qi, B. Zheng, X. Wang, B. Yu, K. Zhou, W. Zhang, Y. Li, and Y. Chen, J. Energy Chem. 26 (2017) 1271.
[29] J. Lu, Y. Zeng, X. Ma, H. Wang, L. Gao, H. Zhong, and Q. Meng, Polymers 11 (2019) 828.
[30] H. Du, Q. Liu, N. Cheng, A.M. Asiri, X. Sun, and C.M. Li, J. Mater. Chem. A 2 (2014) 14812.
[31] X. Liang, B. Zheng, L. Chen, J. Zhang, Z. Zhuang, and B.H. Chen, ACS Appl. Mater. Interfaces 9 (2017) 23222.
[32] S. Li, Y. Wang, S. Peng, L. Zhang, A.M. Al-Enizi, H. Zhang, X. Sun, and G. Zheng, Adv. Energy Mater. 6 (2016) 150166.
[33] L. Fan, P.F. Liu, X. Yan, G. Gu, Z.Z. Yang, H.G. Yang, S. Qiu, and X. Yao, Nat. Commun. 7 (2016) 10667.
[34] X.Y. Yu, Y. Feng, B. Guan, X.W. Lou, and U. Paik, Energy Environ. Sci. 9 (2016) 1246.
[35] B. Wang, X. Bai, Y. Zhu, Y. Zhang, T. Lu, Y. Pan, and J. Wang, Adv. Mater. 31 (2019) 1805658.
[36] W. Wang, X. Xu, W. Zhou, and Z. Shao, Adv. Sci. 4 (2017) 1600371.
[37] H.M. Yang, X.L. Song, T.L. Yang, Z.H. Liang, C.M. Fan, and X.G. Hao, RSC Adv. 4 (2014) 15720.
[38] Y. Li, S. Niu, D. Rakov, Y. Wang, M. Caban-Acevedo, S. Zheng, B. Song, and P. Xu, Nanoscale 10 (2018) 7291.
[39] X. Li, Z. Niu, J. Jiang, and L. Ai, J. Mater. Chem. A 4 (2016) 3204.
[40] J. Qian, F. Sun, and L. Qin, Mater. Lett. 82 (2012) 220.
[41] T. Tian, L. Ai, and J. Jiang, RSC Adv. 5 (2015) 10290.
[42] M. Wang, J. Liu, C. Guo, X. Gao, C. Gong, Y. Wang, B. Liu, X. Li, G.G. Gurzadyan, and L. Sun, J. Mater. Chem. A 6 (2018) 4768.
[43] M. Jin, S.Y. Lu, L. Ma, M.Y. Gan, Y. Lei, X.L. Zhang, G. Fu, P.S. Yang, and M.F. Yan, J. Power Sources 341 (2017) 294.
[44] A. Khan, M. Ali, A. Ilyas, P. Naik, I.F.J. Vankelecom, M.A. Gilani, M.R. Bilad, Z. Sajjad, and A.L. Khan, Sep. Purif. Technol. 206 (2018) 50.
[45] M.S. Rahmanifar, H. Hesari, A. Noori, M.Y. Masoomi, A. Morsali, and M.F. Mousavi, Electrochim. Acta 275 (2018) 76.
[46] S.A. Mousavi and M. Mehrpooya, Anal. Bioanal. Electrochem. 16 (2024) 280.
[47] Y. Tan, J. Feng, H. Dong, L. Liu, S. Zhao, F. Lai, et al., Adv. Funct. Mater. 33 (2023) 2209967.

[48] S.A. Mousavi and M. Mehrpooya, Energy 214 (2021) 119053.
[49] H. Xia, J. Zhang, Z. Yang, S. Guo, S. Guo, and Q. Xu, Nano-Micro Lett. 9 (2017) 43.
[50] J.K. Nørskov, T. Bligaard, A. Logadottir, J.R. Kitchin, J.G. Chen, S. Pandelov, et al., J. Electrochem. Soc. 152 (2005) J23.
[51] Y. Zhang, J. Liu, A. Kumar, W. Chen, and H. Wang, J. Mater. Chem. A 13 (2025) 14567.
[52] Y. Zhang, Y. Liu, Y. Wang, and Y. Li, Mater. Horiz. 10 (2023) 843.
[53] Y. Pei, Y. Cheng, J. Chen, W. Smith, P. Dong, P.M. Ajayan, M. Ye, and J. Shen, J. Mater. Chem. A 6 (2018) 23220.
[54] J.D. Blakemore, R.H. Crabtree, and G.W. Brudvig, Chem. Rev. 115 (2015) 12974.
[55] T. Priamushko, R. Guillet-Nicolas, and F. Kleitz, Inorganics 7 (2019) 98.
[56] Y. Pei, J. Cheng, W. Chen, W. Smith, P. Dong, P.M. Ajayan, et al., J. Mater. Chem. A 6 (2018) 23220.
[57] J.H. Li, Y.S. Wang, Y.C. Chen, and C.W. Kung, Appl. Sci. 9 (2019) 2427.
[58] W. Dai, X. Bai, Y.A. Zhu, Y. Zhang, T. Lu, Y. Pan, and J. Wang, J. Mater. Chem. A 9 (2021) 6432.
[59] H. Liu, X. Ma, H. Hu, Y. Pan, W. Zhao, J. Liu, X. Zhao, J. Wang, Z. Yang, Q. Zhao, and H. Ning, ACS Appl. Mater. Interfaces 11 (2019) 15528.
[60] D. Tyndall, M.J. Craig, L. Gannon, C. McGuinness, A. Roy, M. García-Melchor, M.P. Browne, and V. Nicolosi, J. Mater. Chem. A 11 (2023) 4067.
[61] J. Gupta, D. Das, P.H. Borse, and B.V. Sarada, Sustainable Energy Fuels 8 (2024) 7.
[62] X. Yang, J. Chen, Y. Chen, P. Feng, H. Lai, J. Li, and X. Luo, Nano-Micro Lett. 10 (2018) 15.